Review article

Jangwoon Sung, Gun-Yeal Lee and Byoungho Lee*

Progresses in the practical metasurface for holography and lens

https://doi.org/10.1515/nanoph-2019-0203
Received June 30, 2019; revised August 8, 2019; accepted August 9, 2019

Abstract: Metasurfaces have received enormous attention thanks to their unique ability to modulate electromagnetic properties of light in various frequency regimes. Recently, exploiting its fabrication ease and modulation strength, unprecedented and unique controlling of light that surpasses conventional optical devices has been suggested and studied a lot. Here, in this paper, we discuss some parts of this trend including holography, imaging application, dispersion control, and multiplexing, mostly operating for optical frequency regime. Finally, we will outlook the future of the devices with recent applications of these metasurfaces.

Keywords: flat optics; metamaterial; metasurface.

1 Introduction

The prefix meta- means to transcend the following suffix, which implies that one can think of the optical metasurface as something that surpasses the normal surface. Metasurfaces are different from normal surfaces because light reacts abnormally at their boundary in an unexpected manner [1–13]. Practically, they are composed of artificial subwavelength structures that utilize light-matter interactions for specific purposes. Like metamaterials, the building blocks of metasurfaces are dubbed as meta-atoms, and meta-atoms are engineered to have abnormal electric permittivity and magnetic permeability that are not shown in natural materials. In addition, metasurfaces attract enormous attention thanks to their easier fabrication than metamaterials thanks to two-dimensional shapes [9, 14]. As one can think, the scale of meta-atoms should be smaller than the operational wavelength, so that the early researches on metamaterials or metasurfaces were performed in microwave range, which has a wavelength in centimeter scale [11, 15, 16]. Recent nanofabrication technology makes it possible to manufacture tens of nanometer-scale building blocks on wafer, and this enables to make metasurfaces in the optical regime by scaling down the unit cell of the metasurface, well known as meta-atom. In this regard, this review will concentrate on recent metasurface researches that operates from near infrared to visible range.

Metasurfaces, regarded as future optical components in the recent decade, have been widely studied thanks to their capability of light manipulation within subwavelength thickness. Each meta-atom is engineered to output desired electromagnetic characteristics independently at spatially varied manner. Notably, light manipulation through meta-atom has surpassed the conventional optic components in terms of their compactness as well as their performances [8, 17]. Mostly, this nature has been utilized in abrupt phase discontinuities, generation of desired surface wave, sweeping polarization states with intensity, and creation of desired dispersive properties [18–28]. The metasurfaces first were exploited a lot for the desired wavefront control for the substitution of optic components with high-performance and ultrathin counterparts, such as hologram generation, lensing, and beam router [6, 29–38]. These properties have developed to go beyond the conventional device, such as polarization multiplexing, on-chip plasmonic polarimetry, multiwavelength functionality, and dispersion engineering [19, 22, 39–44].

In this review, we will briefly discuss the principle of optical metasurfaces and review the metasurface holography, which has benefited from the elimination of unwanted diffraction orders and wide viewing angle for three-dimensional (3D) holograms. We will review researches from initial stages of hologram generation

***Corresponding author: Byoungho Lee,** School of Electrical and Computer Engineering and Inter-University Semiconductor Research Center, Seoul National University, Gwanak-Gu Gwanakro 1, Seoul 08826, Republic of Korea, e-mail: byoungho@snu.ac.kr.
https://orcid.org/0000-0002-0477-9539
Jangwoon Sung and Gun-Yeal Lee: School of Electrical and Computer Engineering and Inter-University Semiconductor Research Center, Seoul National University, Gwanak-Gu Gwanakro 1, Seoul 08826, Republic of Korea

to the latest developments. Next, we will review the practical metasurface application, metalens, which is a lens implemented with a metasurface. It covers a wide range of research from early study of focusing light with metasurfaces to recent applications of metalens. Meanwhile, we will also briefly discuss how they make unprecedented light control and are applied in real optic devices.

2 Metasurface holography

Holography, in its broadest sense, refers to the optical technique of controlling the wavefront of light as desired by spatially varied change of phase and amplitude [45, 46]. Previously, in order to reproduce a hologram through the spatial light modulator, it is indispensable to have a pixel pitch that reaches up to micrometer scale and corresponding sampling problems that needs improvement in image quality [47, 48]. However, in the case of a metahologram, which indicates the holography produced by a metasurface, the problems regarding large pixel pitch vanish thanks to its subwavelength periodic length. This is because each meta-atom contains information of the phase or amplitude of light [1–20]. In this section, we discuss how light reacts with meta-atoms and review some of the representative metahologram studies together.

2.1 Early metasurface holography

Early metahologram studies exploited the Pancharatnam-Berry (PB) phase control method, also called geometric phase [29, 31, 32, 39, 49–51]. This PB phase is based on a principle that phase retardation of the scattered cross-polarization component is determined by the in-plane orientation angle of the meta-atom. As shown in Figure 1A, the incident light should be circularly polarized light, and PB phase applies to both the cross-polarized components of reflection and transmission. It can be simply expressed by the Jones matrix as follows in regard of transmitted light:

$$T = \Lambda R(-\theta)\begin{bmatrix} t_{xx} & 0 \\ 0 & t_{yy} \end{bmatrix} R(\theta)\Lambda^{-1} = \begin{bmatrix} t_{xx}+t_{yy} & (t_{xx}-t_{yy})e^{i2\theta} \\ (t_{xx}-t_{yy})e^{-i2\theta} & t_{xx}+t_{yy} \end{bmatrix} \quad (1)$$

where Λ is a transformation matrix from the linear polarization basis to circular polarization and $R(\theta)$ is a rotation matrix. t_{xx} and t_{yy} are the transmission coefficients from a meta-atom: t_{xx} is the x-polarized transmission coefficient when incident light is an x-polarized light, and t_{yy} the is the y-polarized one when a y-polarized light is incident. As seen from Equation (1), unlike other phase modulation methods to be described, it has the advantage that it is not wavelength selective. The initial metahologram studies can be seen in Figure 1B and C [29, 49]. Hence, the

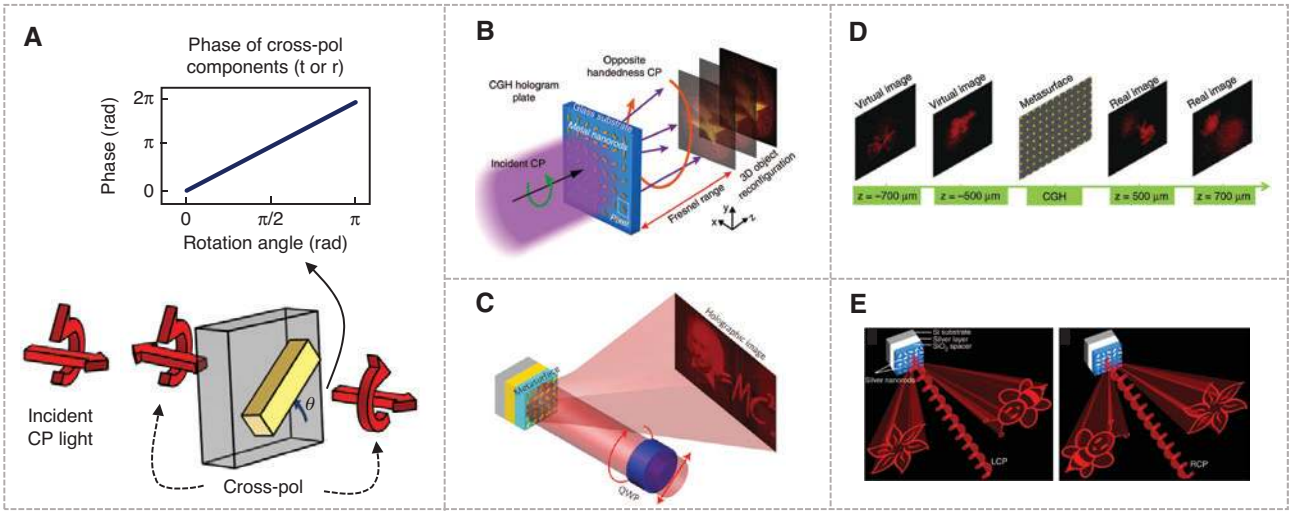

Figure 1: Phase modulation methods with meta-atoms and metahologram examples.
(A) Schematic diagram showing the mechanism of the PB phase method (bottom) and the graph of resultant phase value of the scattered cross-polarized component. (B) Transmissive-type three-dimensional optical holography by plasmonic metasurface [29]. (C) Reflective-type hologram reaching 80% efficiency with plasmonic metasurface [49]. (D) Holographic multiplexing via plasmonic metasurfaces [50]. (E) Reflective-type helicity multiplexed meta-hologram [39].

meta-atoms consist of metal scatterers, and the metasurfaces that are composed of metal meta-atoms are called plasmonic metasurfaces. To avoid low efficiency, they are typically designed to operate in infrared or longer wavelength regime. Here, the hologram generation methods used in Figure 1B and C are different from each other. In the case of Figure 1B, the hologram image is reproduced in the Fresnel range from the position of the metasurface. That is, it can contain information according to the depth of the image, so it is also called 3D holographic image. Conversely, the holographic image shown in Figure 1C is reproduced in a Fraunhofer region. This can be obtained through the Gerchberg-Saxon algorithm, which is a method of generating phase information to reproduce a hologram at the Fourier distance. The resultant phase mask is called a computer-generated hologram (CGH). As a result, there are two ways to reproduce the hologram through the metasurface. In addition, when the handedness or helicity of the circularly polarized light is changed, the sign of the PB phase is flipped, as shown in Equation (1). In other words, the PB phase converts to the opposite sign when the handedness of the incident light is reversed. Figure 1D and E show two applications of this method to the holographic multiplexing [39, 50]. Figure 1D shows the case where the CGH is designed for holographic multiplexing. The four different images are recorded in one CGH with various imaging depths. Here, note that the images of which the imaging depth is in negative sign are virtual images, and this can be applied in holographic multiplexing as follows: If the helicity of light is altered, the real image of rabbit is replaced into the bear image, which was a virtual image having the same distance from the metasurface before the helicity reversal. Therefore, if the image is measured at $z = 500$ μm, two different holographic images can be obtained by varying the handedness of polarization. Figure 1E shows an example of holographic multiplexing through the Fourier hologram. When the helicity of the incident light is reversed, the Fourier image is inverted in terms of the coordinate of the image, as shown in Figure 1E. It is notable that both methods shown in Figure 1D and E implement multiplexing by a single CGH, which means recording more than one CGH is not achievable with these methods.

2.2 Metasurface holography with more-than-one information

The study of metasurface holography has been carried out to increase the amount of information on one metasurface. This method is made possible by using a new structure, controlling the properties of incident light, or using a reflection space as modulating range with transmission space [21, 52–59]. The phase control via PB phase is well known to have a broadband characteristic [21, 29, 51]. However, if the resonant characteristic is added to the meta-atom for addition of auxiliary functionality or subsidiary information, the broadband operation becomes impossible [19, 52, 54]. Consequently, broadband-operating metasurfaces that can function beyond single phase control have also been studied [21, 60–62].

As anisotropy is induced in the asymmetric molecular structure of nature, the asymmetric geometry of the meta atom can also give anisotropy as shown in Figure 2A. Accordingly, anisotropic meta-atoms have been developed to apply different phases in orthogonal linear polarizations. Unlike the PB phase, which is a method using structures of the same shape and size, the shapes of the meta-atoms should be different in order to elicit different reactions for two mutually orthogonal polarized light [20, 63]. This was made possible by changing the shape of the plasmonic structures (Figure 2B) [63]. This method is based on the fact that an abrupt phase discontinuity occurs depending on the resonant characteristics of the plasmonic structure. As the shape of the meta-atom can be freely adjusted within the constraint of fixed thickness, the metasurface can have spatially varying anisotropy. This allows polarization multiplexing in terms of phase control.

Another phase modulation method is possible for polarization multiplexing, which is detouring phase delay by arrangement of meta-atom [64]. Assuming that the meta-atoms are arranged in sufficiently long periodicity for the generation of diffraction order and the image is captured from the plane perpendicular to the diffracted angle, the phase difference between two adjacent meta-atoms will be zero. Here, when one of the meta-atoms is moved horizontally as shown in Figure 2C, the phase difference occurs as result, which is $kd \sin\theta$, where k is the wavenumber of incident light and θ is the diffraction angle. As a result, it is possible to introduce an additional degree of freedom in phase modulation. Figure 2D shows the polarization multiplexing result when the phase detouring is combined with the PB phase [54]. As shown in Figure 2D, as the helicity of the incident light is altered, the reproduced CGH is flipped into the other one.

In the case of the hologram through the plasmonic metasurface, there is a inherent problem in that the hologram conversion efficiency becomes low when it is made into a transmission type. This can be solved with a metasurface through a dielectric with high refractive index and low extinction coefficient. The principle is as follows: For a meta-atom of sufficiently high thickness, the effective

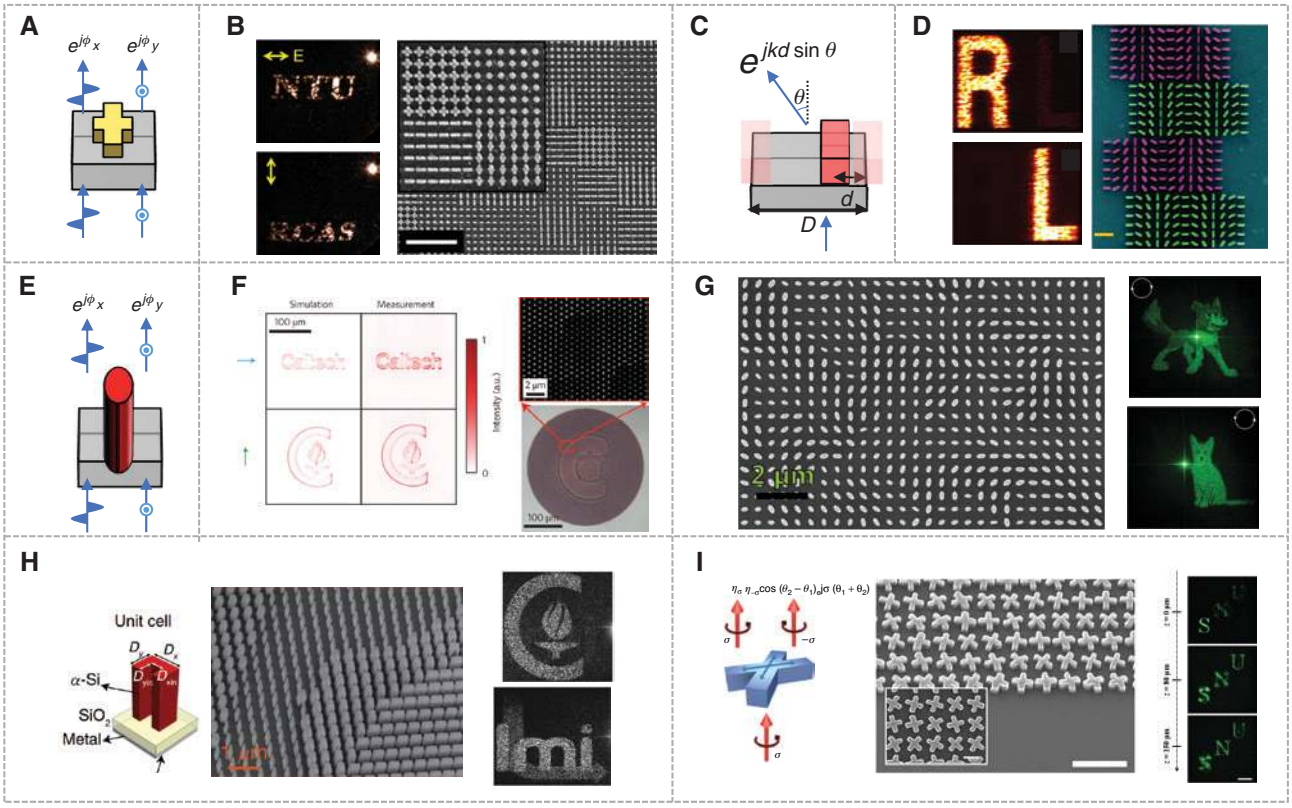

Figure 2: Meta-hologram multiplexing.
(A) Schematic diagram of anisotropic resonant plasmonic meta-atom. The light scattered by this meta-atom becomes to get distinctive phase values according to the polarization states of incident light. (B) Polarization-controlled dual holographic images by anisotropic plasmonic metasurface [63]. The left images show the experimental result by polarization, and scanning electron microscope (SEM) images are shown on the right side. Scale bar is 2 μm. (C) Schematic illustration for the explanation of the detoured phase. As mentioned in the text, phase values are determined by the displacement parameter *d* of each unit cell. (D) Broadband and chiral metaholograms dependent on the handedness of incident light [64]. On the left are the camera-captured images by polarization handedness (right for upper, left for lower image). On the right is the SEM image of the fabricated sample. The scale bar is 1 μm. (E) Schematic diagram of dielectric meta-atom, which imparts a distinguished phase in accordance with the polarization state. (F) Dielectric metasurfaces for the control of phase and polarization with high transmissive efficiency [20]. On the left, the resultant simulation and experimental results are shown for two polarizations. On the right, the SEM images and captured image by optical microscope are shown. (G) Independent phase control of arbitrary orthogonal states of polarization by TiO_2 metasurface [19]. Figures are one example of which the basis is circular polarization. The left image shows the captured holographic images. The sign depicted on the corner of figures indicates polarization of incident light. The SEM image of this fabricated sample is shown on the right. (H) Angle-multiplexed metasurface for independent phase profile under different incident angles [55]. The two images on the right are captured holographic images at different illumination angles. (I) The X-shaped metasurface for complete amplitude and phase control of light [21]. The right three images are captured by charge-coupled device camera with varying longitudinal position.

refractive index varies with the size that occupies a unit cell, and by its index, the phase can be modulated up to 2π [2, 7, 20, 65]. These all-dielectric metasurfaces have merits on transmission efficiency but are less advantageous in thickness than plasmonic metasurfaces. Usually the all-dielectric metasurfaces have thickness similar to the operating wavelength, while plasmonic metasurfaces have thicknesses much smaller than that.

As shown in Figure 2E, the dielectric meta-atom has an anisotropic shape, which in turn contributes to birefringent characteristics. This is exploited to birefringent phase control in Figure 2F, which has near 100% diffraction efficiency in two different polarization states at near-infrared wavelength. Each of the silicon meta-atom has spatially varying size parameters in both *x*- and *y*-directions, and this is attributed to the full phase modulation of both polarization states. In terms of the two degrees of freedom of ellipse size, it is possible to produce two independent phase profiles of t_{xx} and t_{yy}. Until recently, this method has influenced almost all of the studies of polarization multiplexing metahologram including the study in Figure 2G [20]. As it is possible to realize independent phase control with unity efficiency, $t_{xx}-t_{yy}$ can be freely expressed as $e^{i\phi}$, by simple tuning of

size parameters. Therefore, in circular polarization basis, cross-polarized components can be combined with the PB phase to become dependent on the helicity, which can result in the imparting of two independent phase masks. Capasso's group showed that, through the studies in Figure 2G, fine-tuning of size and in-plane rotation angle of the meta-atom contributes to create two independent phase profiles based on all orthonormal basis of polarization [20]. As this mechanism employs the titanium dioxide meta-atom of which efficiency is up to 100% in visible frequency, no polarizer is needed at the output terminal. Thanks to the efficient nature of dielectric metasurface, the meta-atom was designed to impart distinct phase retardation by the incident angle, that is, the direction of the incident light [55, 56, 66–68]. In Figure 2H, the shape of the structure is carefully adjusted to impart a different phase according to the incident angle [55]. While conventional metaholograms are mostly concentrated on phase-only hologram, the hologram that is reconstructed from the phase and amplitude together is desirable. In this regard, Figure 2I shows the independent and continuous modulation of the amplitude and phase in broadband through the X-shaped meta-atom [21]. This enables broadband characteristics by extending the PB phase and a remarkably low noise-to-signal ratio compared with conventional phase-only holograms thanks to the capacity of X-shaped meta-atom, which carries amplitude and phase information together.

2.3 Full color metahologram

Wavelength multiplexing or full color metaholograms have been studied in various ways [40, 66–75]. When recording CGH, setting fixed image plane with incident angles by wavelengths can enable the full-color holography. For example, as shown in Figure 3A, for green light, CGH is generated assuming the letter G is put in the center of the image plane [67–69]. Next, for red and blue lights, the angle of incidence is set in advance, then the CGH is calculated so that the letter (or image) can be generated at the predetermined image plane. In this way, the desired color image is retrieved only by the predetermined incident angle varied by wavelengths. This scheme has been applied in other color hologram as well, covering full-space color holography, which shows independent

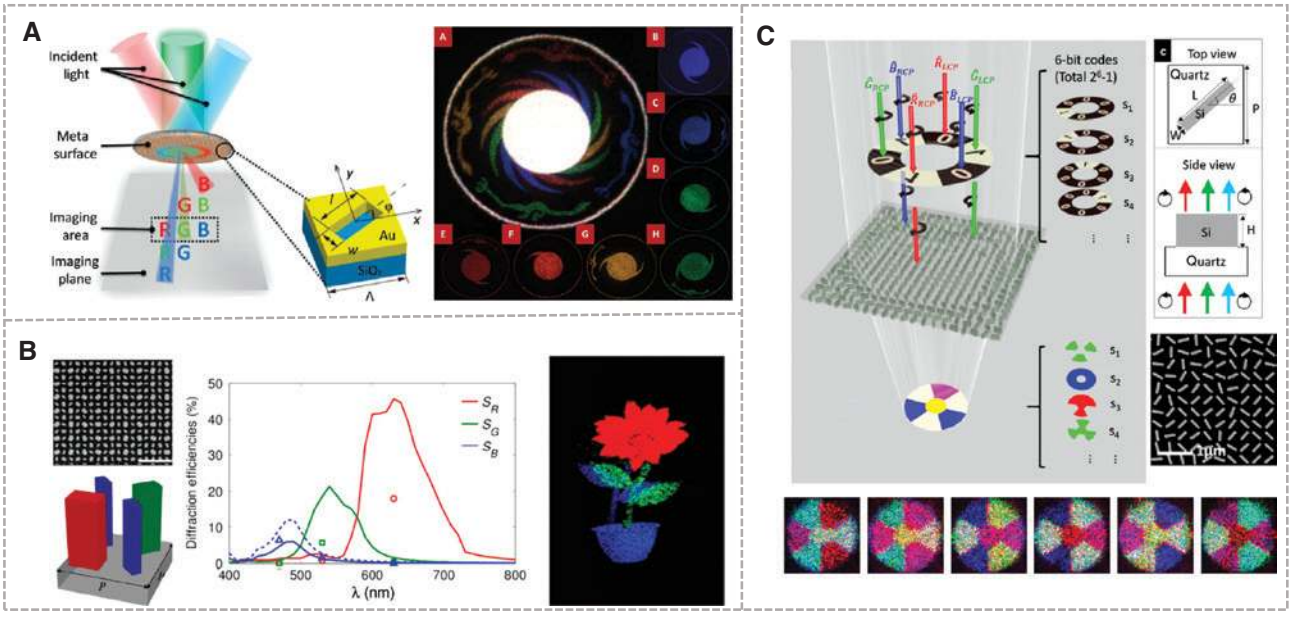

Figure 3: Multicolor metaholograms.
(A) Multicolor 3D metaholography by broadband plasmonic metasurface [69]. The left shows the conceptual illustration for understanding the scheme to achieve multicolor hologram. On the right is the measured holographic image that accomplished seven colored holographic image. (B) Dielectric metasurfaces for multiwavelength achromatic hologram for three wavelengths [40]. SEM image is shown on the top left, and the scale bar is 1 μm. Bottom left shows the unit cell of the proposed structure, and the graph indicates the mechanism of this metasurface: Each colored meta-atom contributes to the phase modulation of the color wavelength itself. The right image is the experimental result. (C) Noninterleaved metasurface for 2^6-1 spin- and wavelength-encoded hologram [70]. The top left image shows the operational principle of the proposed scheme. On the right, the top and side views of the unit structure are shown as well as the SEM image of fabricated sample. The bottom six images are the measured result of the achieved wavelength- and spin-encoded holographic images.

colored images simultaneously in transmission and reflection space [66].

The method used in Figure 3B is to generate the wavelength-selective properties via adjusting the size of the structure and then to intersperse all the structures with one unit cell [40, 76–79]. Each meta-atom has a well-reacting wavelength according to its sizes in visible region. This makes possible to construct three independent CGHs for the three structures, and consequently, three CGHs, which have wavelength information as well, can be imprinted with one metasurface. The result can be seen in Figure 3B, and crosstalk is inevitable because each meta-atom is not completely wavelength selective [40].

Full color holograms can also be implemented by recording many holographic images of different depths in a single CGH [70]. As shown in Figure 3C, this scheme is realized by the PB phase and utilizes the fact that virtual images that can be measured by looking inside the metasurface can be changed into real images simply by altering the helicity of polarization [70]. In addition to this, this scheme employs the diffractive characteristic of the metasurface of which the propagated position where the holographic image is generated increases by blue shift of wavelength. As a result, with image plane fixed and wavelength and polarization shifted, the number of 2^6-1 images are multiplexed with non-interleaving metasurface.

2.4 Tunable metasurface holography

In the case of the metaholograms so far, the phase mask recorded in the metasurface cannot be changed into other information once it has been fabricated. To address these limitations, some of the recent published studies have proposed dynamic metaholograms using various methods [60, 80–83]. When a meta-atom is designed using a material whose permittivity changes by external bias, the metasurface can contain more than one information without change of incident light properties. In the optical frequency domain, well-known phase change materials such as vanadium oxide, liquid crystal, indium tin dioxide (ITO), and GeSbTe (GST) based materials have been actively employed as dynamic nanophotonic devices so far [60, 80, 84–88]. Especially, GST is a material whose state changes from amorphous into crystalline and vice versa according to external stimuli such as thermal or electrical bias [89, 90]. In the study shown in Figure 4A, GST is used as ultrathin substrate that reacts resonantly with plasmonic metasurface to be utilized as dynamic metadevice [80]. This is applied in metahologram in the manner that the holographic image is reproduced only in the amorphous state, and in crystalline state, only meaningless information is retrieved. In Figure 4B, the GST nanostructured metasurface is designed in a C-shape to impart two CGHs according to the states [60]. Two sizes of meta-atom are used to realize amplitude extinction at both states. This scheme is also used in other studies including research at Figure 4C (not in a chronological order) [81, 82]. In addition, novel external biases using hydrogen and oxygen are also presented. As can be seen in the figure, this study using the state change of magnesium with the air is used as holographic image encryption or dynamic Janus hologram. A tunable metahologram can be realized using the materials changed by mechanical stimuli. As shown in Figure 4D, the study used PDMS, which is a stretchable material, as a substrate for realization of a tunable hologram [91]. This study utilizes the fact that the image plane changes as the periodicity is tuned.

2.5 Recent metasurface holography technology

Recently, metasurface holography technology has been developed further to achieve unprecedented light control by novel meta-atom designs. Here, we introduce six representative examples, which accomplish improved versatility. The structure in Figure 5A is designed in the same way as the one proposed in Figure 2F [20, 52]. However, in addition to recording two different CGHs using the PB phase and the fact that t_{xx} and t_{yy} can be controlled in Equation (1), one CGH is additionally recorded through the novel algorithm. On the basis of linearly polarized light, additional CGH is recorded in t_{xy} (or t_{yx}). On the basis of circular polarization, two CGHs are recorded in cross-polarized components according to handedness of incident light, and the other one is added to the co-polarized component. As a result, three different CGHs are imparted with a single metasurface at the optical frequency.

Some studies have been made to control light in transmission and reflection space together [42, 53, 54, 66, 92–94]. For instance, the structure shown in Figure 5B takes advantage of the fact that incident light is reflected when two transmitted lights are out of phase in the range where no diffraction order occurs [53]. Both meta-atoms used in this paper are designed to act as perfect half-wave plates for high efficiency. Through a combination of two engineered meta-atoms, asymmetric transmission controlled by handedness is implemented, and by the in-plane rotation angle of the whole structure, phase modulation is achieved as well. Furthermore, as shown in Figure 5C, a bifacial metasurface has been designed to impart different

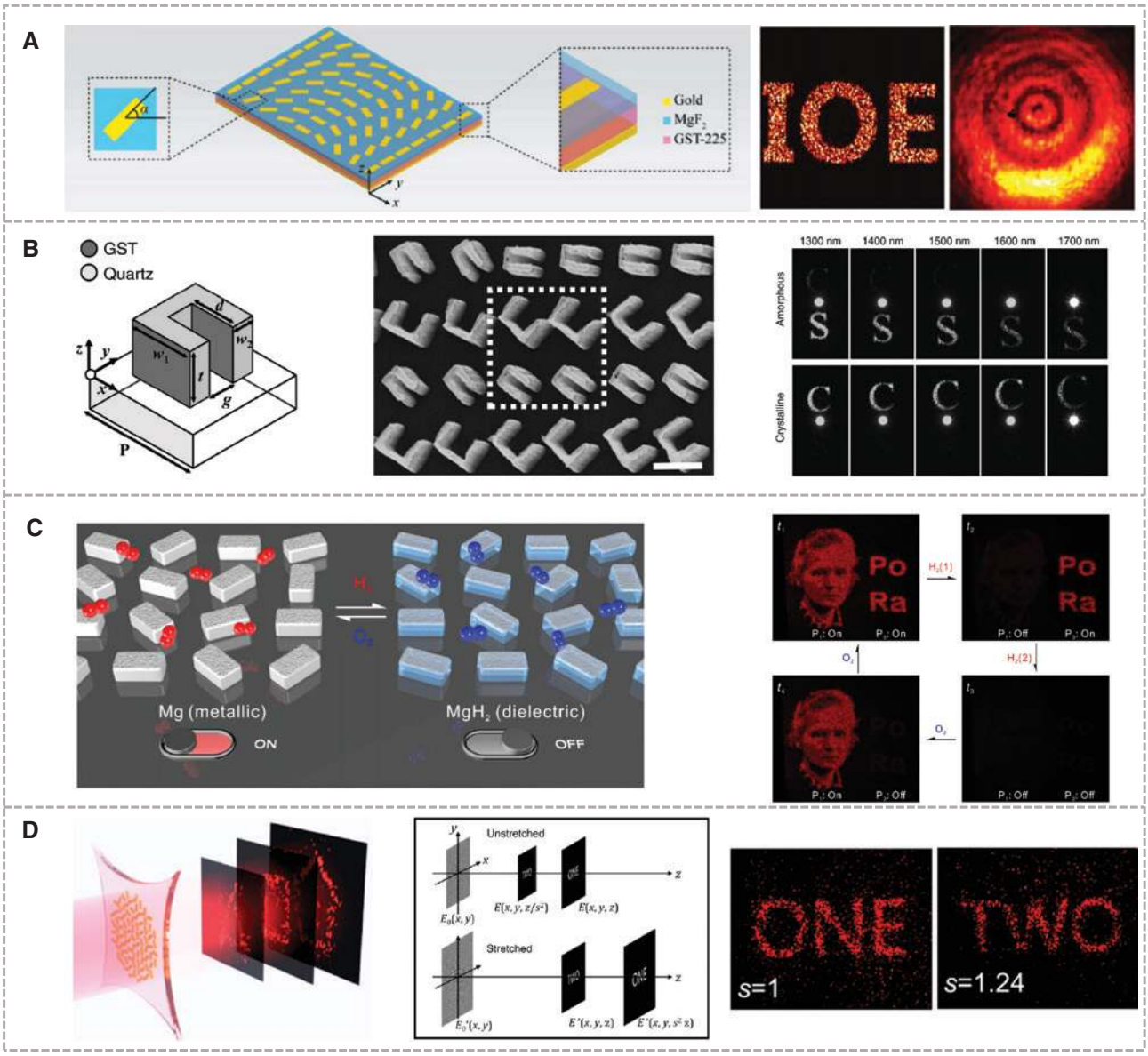

Figure 4: Tunable and dynamic metahologram.
(A) Plasmonic metasurface for switchable photonic spin-orbit interactions based on GST [80]. The left image shows the material and schematic diagram for the proposed structure. The right two images are captured holographic images from the fabricated sample, which only show the operation on the amorphous state of GST. (B) GST-nanostructured metasurface for wavefront switching [60]. The left image shows the C-shaped meta-atom for the unit cell of the proposed structure. The middle image shows the SEM image of the sample. Scale bar is 500 nm. The right images are measured results according to the states of GST meta-atom and selected wavelengths. (C) Addressable metasurfaces for dynamic hologram and optical information encryption [81]. The left image shows the mechanism of proposed plasmonic metasurface. The right shows how the holographic image from the proposed structure can be dynamically tuned by hydrogen and oxygen. (D) Strain multiplexed metasurface hologram by stretchable substrate [91]. The left and middle images show the schematic of the proposed scheme. The two images on the right are captured holographic images by varying the pulling force to substrate.

CGHs in the transmission and reflection spaces simultaneously [54]. In addition to creating the same PB phase in the transmission and reflection spaces, independent phase control is achieved by controlling the phase difference between the two spaces by spatially varying the size of the meta-atom. Unlike the studies that accomplish the full-space control in the gigahertz region, the bifacial metasurface is composed of a single-layer silicon meta-atom and operates in the visible range.

As shown in Figure 5D, a coherent meta pixel has been introduced in which the observed image is changed by the angle, wavelength, and polarization of

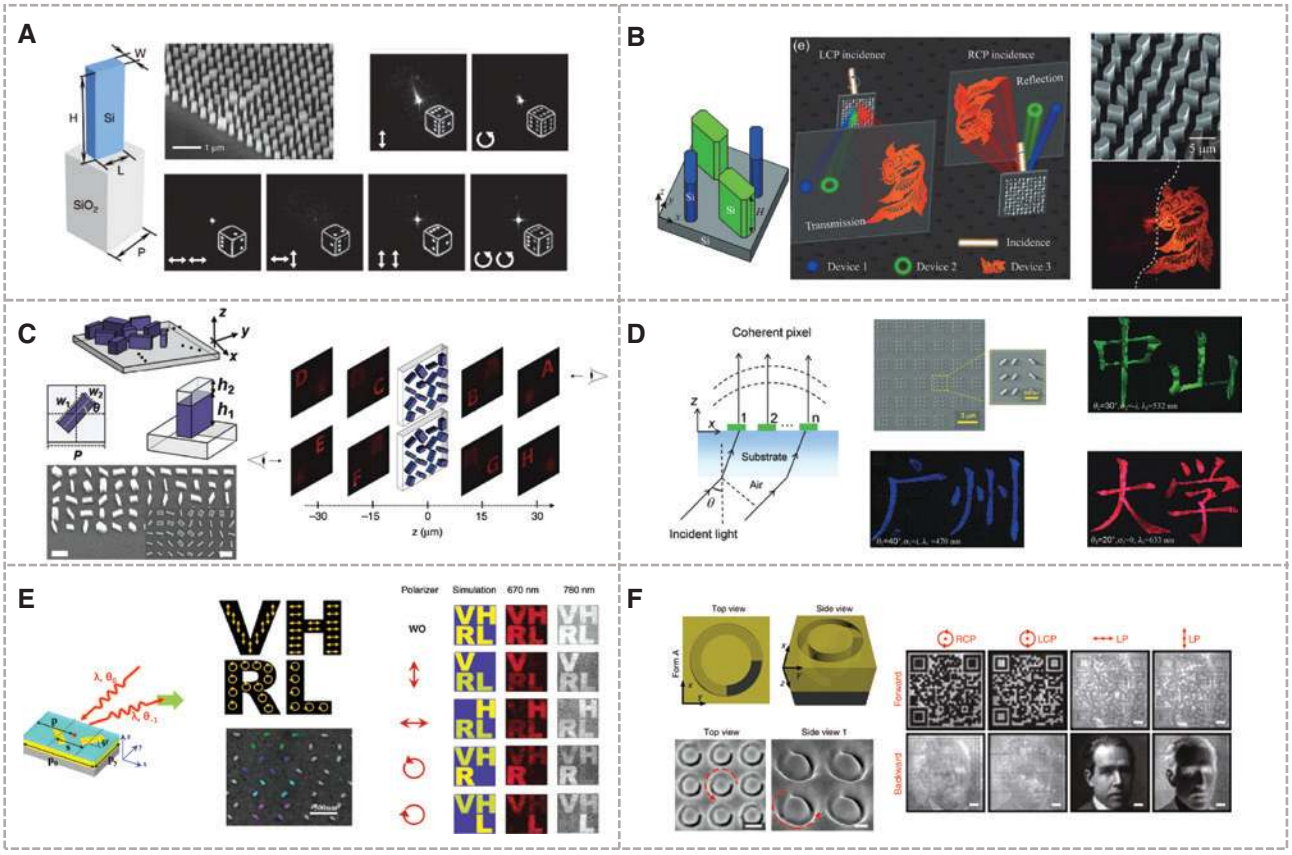

Figure 5: Recent advances on the metasurface-based holography.
Each figure is arranged in order of schematic diagram of the proposed structure, SEM image, and experimental result. (A) Multichannel vectorial holographic image and encryption [52]. Regarding the experimental result, the upper two images are captured images varying incident polarizations with no polarizer at the output terminal. Lower four images are captured with polarizer: the left indications are incident polarization, and the right indicates the filter used before measurement. (B) Simultaneous circular asymmetric transmission and wavefront shaping by dielectric metasurfaces [53]. The left figure shows the unit cell structure. (C) Bifacial metasurface for independent phase control on transmission and reflection spaces [54]. The right figure shows the generated holographic image that is differently reproduced by viewing direction. (D) Coherent pixel design of metasurfaces for multidimensional optical control of multiple printing-image switching and encoding [56]. Right three resultant images are obtained by different wavelength, polarization, and incident angle. (E) Diatomic metasurface for vectorial holography [57]. The top middle figure is the desired vectorial holographic image that possesses intensity and polarization information as well. The lower image is the SEM image for the sample. The right figures are measured images, which shows a great match with the simulation results. (F) Plasmonic helical nanoapertures for 3D Janus polarization-encoded image [58]. The right figures are measured images from different illuminated directions with distinct polarization.

the incident light [56]. This coherent pixel scheme is meaningful because it is possible to confirm the multiplexed image by freely choosing the area to reproduce the image, unless it is measured with high-NA system. Similarly, some studies have been proposed, based on the fact that when the spectral characteristic, phase, and polarization state of a meta atom are different from each other, it is distinguished when observed in bare eye or optical microscope [73].

As the reflective plasmonic metasurface, a novel concept of holography based on two orthogonal meta-atoms is proposed in Figure 5E [57]. This method enables vectorial holography, which can realize holography having the spatially varying polarization state and amplitude. In addition, as shown in Figure 4H, a plasmonic metasurface can be obtained by milling a metal plate while controlling the concentration of the focused ion beam [58, 62]. The resultant meta-atom breaks mirror symmetry, which is not achievable with fixed height and planar meta-atom [95–98]. This leads to the chiral response to the circular polarization, and some studies employ this scheme to realize polarization-dependent image generation. The study shown in Figure 5F achieves polarization-controlled Janus image, by control of the extinction ratio of the amplitude by changing the incident light direction and polarization [58].

3 Lensing with metasurfaces

3.1 Metalens: lens made of metasurface

Recently, the commercial market for head mounting type devices such as augmented reality (AR) and virtual reality (VR) is increasing, and as the importance of lightness and compactness of devices such as cameras and optical sensors used in smart phones emerges, a demand for a new platform is increasing [99–101]. Through the Fresnel lens, or Echelette-type lens, the thickness of the lens can be reduced, but in spite of their potential, such a lens has problems such as the reduction of light efficiency compared with shadow effects [6, 102]. Conversely, by using a metasurface as a planar lens, ultrathin characteristics as well as no shadow effect can be accomplished [30, 31, 103–106]. In terms of development potential, research has been conducted in various directions to utilize the metasurface as a lens by the unprecedented light control ability of the metasurface.

Metalenses are often made of dielectric materials because their efficiency is important for imaging through the lens [30, 105]. Of course, similar to holography, the early metalens, which operates in the visible light band, is a plasmonic structure, so that it suffers from significantly low conversion efficiency considering practical imaging applications where efficiency is highly an important component [107–111]. To solve this efficiency issue, plasmonic metalenses have often been designed as reflective types or in sparsely arranged manner similar to Fresnel zone plate [112–115].

As in the previous holographic reproduction, when designing the lens through the metasurface, the phase adjustment at the subwavelength pixel is required: A metalens is created by imparting a phase profile with a parabolic shape [30]. The phase modulation method is not much different from the previous one. The metalenses shown in Figure 6A and B were designed through the PB phase [30, 31]. The metalens designed through the PB phase has the same size and shape of all the structures, and it is possible to control the phase continuously by adjusting the in-plane angle. In the case of the lens made with diffraction grating in Figure 6A, it is designed to operate in the mid-infrared region, and its diffraction

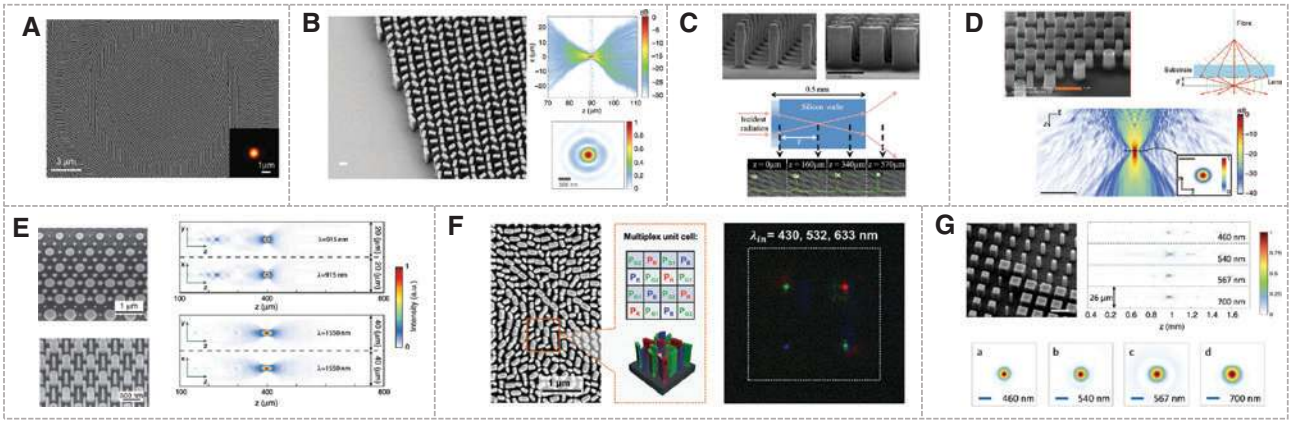

Figure 6: (A–D) Early proposed dielectric metalenses [30, 31, 65, 116].
(A) Dielectric gradient optical elements [31]. High-index dielectric gratings using the PB phase are arranged to achieve the lens phase profile. The inset shows the intensity profile at focus. (B) Visible wavelength metalens for diffraction-limited focusing and subwavelength resolution imaging [30]. The left image shows the SEM captured TiO_2 metalens. The right two images are the measured intensity profile near the focal points. The upper images are captured at the plane that contains the propagation direction vector and the lower plane is perpendicular to the propagation direction. (C) All-dielectric subwavelength focusing lens [116]. The upper images are SEM images from the fabricated sample. The lower images are showing the schematics and the measured intensity profiles of various positions. (D) Subwavelength-thick lenses with high numerical apertures and large efficiency based on high-contrast transmitarray [65]. The upper left image shows the tilted SEM image of transmitarray. The right images show the schematics of the proposed transmitarray. The lower image shows the intensity profile of the proposed structure. (E-G) Metalenses for multiwavelength operation [72, 76, 77]. (E) Multiwavelength polarization-insensitive lenses based on dielectric metasurfaces with metamolecules [77]. The left two images are the top view and the tilted view of the metasurfaces captured by SEM. Right intensity profiles are described as simulation (top) and experimental results (bottom) and detached by wavelengths. (F) Gallium nitride metalens for color routing [76]. The left images describe how the building blocks are made of, and the SEM images are shown as well. The right figure shows the experimental result of which the focal points are distinct in transverse direction. (G) Titanium dioxide metasurface for multiwavelength functions [72]. The upper left image is the tilted view of the fabricated sample. The remnant images show the measurement result of the multiwavelength lens.

efficiency reaches almost 100% [31]. Designed as a thick titanium oxide nanopillar, the meta-atom in Figure 6B is designed to operate in the visible range, with a maximum focusing efficiency of 86% when the NA is 0.8 and the operating wavelength is 405 nm [30]. In the case of the metalens shown in Figure 6C and D, it is made by using the phenomenon that the effective index increases according to the size [65, 116, 117]. These nanoposts are made of amorphous silicon, which are designed to operate in the near-infrared range, and the focusing efficiency is 82%. Unlike the PB phase-based metalens, the metalens operates independently of the polarization because the phase is adjusted according to the size of each meta-atom.

Like the way that metahologram progresses, the metalens has also been developed to have multifunctionality as well [118–123]. For instance, the metamirror has been proposed to focus light with respect to linear polarization by plasmonic metamirror [118]. This scheme utilizes the birefringent resonant characteristics of spatially varying sizes of plasmonic meta-atom. Also, by designing the phase mask as dependent to helicity by PB phase meta-atom and spatial multiplexing, some studies achieve multifocus metalenses [119, 121, 124].

3.2 Metalens research progress: from multiwavelength to tunability

While the metalens has the advantage of being extremely thin compared with the conventional optical element, the effective index-based metalens has a disadvantage that the operating wavelength is limited to a single frequency and coma aberration is severe with respect to the incident angle [65, 116, 117]. To solve these problems, metalenses have been studied in various manners so far. For example, to compensate for chromatic aberration through an existing refractive optics-based lens, various shapes of lenses should be stacked, which results in a bulky system. In the early days, this is solved through the proper design of the metalens, as did the full color metahologram [72, 76–79]. In the metalens of Figure 6E, each meta-atom is designed to operate in different wavelengths of 915 and 1550 nm, respectively, and the two meta-atoms are spatially multiplexed as one unit cell, dubbed as metamolecule [77]. It can be designed to have different phase masks for two wavelengths, and the proposed metalenses are made to have the same focal point. The metalens, shown in Figure 6F, uses a similar scheme as the metamolecule, by designing three meta-atoms that respond to three wavelengths each, like Figure 3B [40, 76]. In this case, the material used is gallium nitride, and as the absorption coefficient in the visible light band is 0, like titanium oxide or silicon nitride, it is possible to design the metalens with high efficiency. In this study, color routing is achieved by imprinting the light in different transverse directions for each wavelength. In the case of the metalens shown in Figure 6G, unlike the previous studies, it is not made by spatial multiplexing of meta-atoms [72]. This metasurface utilizes guided mode resonance, which is a resonance caused by the size of meta-atom, and leads to independent phase modulation for the three different wavelengths. If there is no aberration for only the three most main wavelengths of red, green, and blue lights, it can be applied in optical devices based on tricolor wavelengths, for example, optical elements in VR or RGB-type display.

However, in order to use the metalens as a practical lens for real life or AR, phase imparted from each meta-atom should be changed in nondispersive manner for continuous spectral band. This can be resolved through dispersion engineering through the design of the meta-atom [18, 22, 112, 125–127]. The method shown in Figure 7A is a reflection-type metalens that adjusts the diffractive characteristics of the metasurface, which enables to control not only the phase information but also the wavelength derivative in the near-infrared band [22]. This achieves a dispersionless focusing mirror at a wide bandwidth of 140 nm. After, a study of achromatic metalens for about 500 nm bandwidth by designing several reflective plasmonic meta-atoms was proposed in the infrared region [112]. In this case, each meta-atom has a distinctive frequency derivative that mainly contributes to correct the chromatic aberration, and at the same time, the PB phase is used for the imparting of lens phase profile. This scheme is applied to the visible light band by dielectric meta-atoms as shown in Figure 7B and C [125, 126]. In both studies, the group delay or dispersion was controlled by changing the shape or size of the meta-atom, and the phase was controlled via the PB phase. This provides a basis for eliminating chromatic aberration for circularly polarized light, thus opening up the possibility that metalens can actually be applied with a certain degree of numerical aperture. Recently, a metalens that operates independent of polarization has been designed, as shown in Figure 7D [128]. It basically uses the PB phase, but by using the meta-atoms that are tilted at 0° and 90°, the handedness-dependent property is vanished [128]. Next, the dispersion characteristics and phase are adjusted by the size and shape of each meta-atom, which is composed of more than one nanopillar.

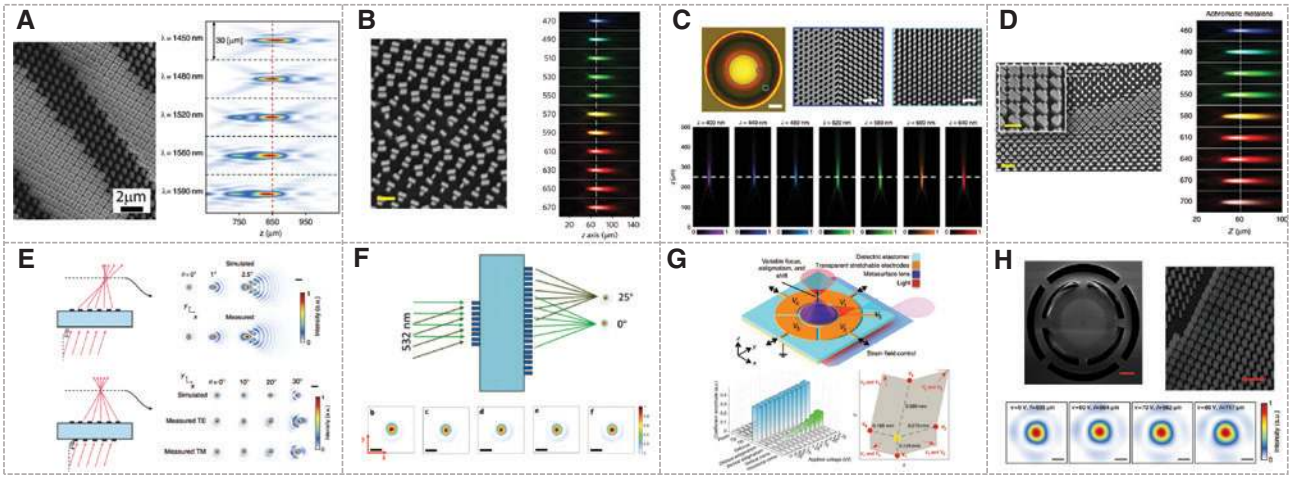

Figure 7: Metalenses for correction of intrinsic aberrations (A–D).
One is the fabricated sample, and the other is the representative result of achromatic metalens, showing intensity profile with distinct wavelengths. (A) Dielectric metasurfaces for control of the chromatic dispersion in near-infrared region [22]. (B) TiO_2 and (C) GaN metalens for achromatic focusing in the visible spectrum using the PB phase with designer meta-atoms [125, 126]. (D) Polarization-insensitive metalens operating in visible frequency [128]. (E–F) Metalens doublet corrected for the monochromatic aberrations [129, 130]. (E) The left two figures for schematic and corresponding right figures imply the difference in aberrations, which is severe at singlet (top), while it is improved in the doublet case (bottom). (F) The left figures show the mechanisms, and the right shows the measured results regarding illumination angle. (G–H) Representative tunable metalenses [131, 132]. (G) Adaptive metalens that can tune the focal point and astigmatism as well [131]. The upper image shows the brief mechanism of the proposed structure, and the lower graphs show the performances. (H) Metalens integrated with micro electro mechanical systems (MEMS) for focal length control [132].

The metalens has a coma aberration that is not suitable for imaging, which was considered to be a major obstacle to real-life application of the metalens. Figure 7E and F show the doublet metalens as a basis for solving this problem [129, 130, 133]. Two doublet metalenses differ from each other in two ways: First, the wavelength bands on which the metalens operates are different, one for the near-infrared band (Figure 7E) and the other for the visible band (Figure 7F) [129, 130]. The second is that the former is based on the size-based phase control, while the latter utilizes the PB phase. In the case of the conventional metalens, the point spread function is greatly distorted even at an incident angle of about 2.5°, which indicates that the coma aberration is serious. However, with doublet metalens, it can be seen that the aberration is greatly reduced even when the light is incident at an angle of 30°.

As in the study on metahologram, several studies have been introduced to control the characteristics of the metalens through external bias [131, 132, 134–137]. Figure 7G and H show two representative examples of tunable metalens [131, 132]. The metalens in Figure 7G can be controlled by a total of five electrical voltage biases through which the focal point and astigmatism can be controlled by the transparent stretchable electrodes [131]. It is meaningful to adjust the focus not only in longitudinal direction but also in the transverse direction as well as its astigmatism. In the case of Figure 7H, the basic principle is similar to the classic zoom lens [132]. It is composed of one metalens on substrate and the other one moving on the membrane. In theory, the optical tunability can be increased to over 300 diopters for the proposed design. Considering the performance of the proposed scheme, the future potential of metalens is well demonstrated numerically and experimentally with this research.

3.3 Researches on the applications of metalens

The metalens has been expected to contribute to the miniaturization of the optical instruments as it can contain much more information than conventional lenses or optic components [99, 133, 138–150]. Figure 8A shows an example of metalens that used the property of the PB phase: The sign of the PB phase is reversed according to the handedness of the incident light [122, 144]. For instance, if a PB phase-based metalens is made to focus light for left-handed circularly polarized light, it operates as a diverging lens for the right-handed circularly polarized light. That is, if a phase mask that operates for the left circularly polarized light and right circularly polarized light together can be formed with one metasurface and the focus positions of the two lenses are made different

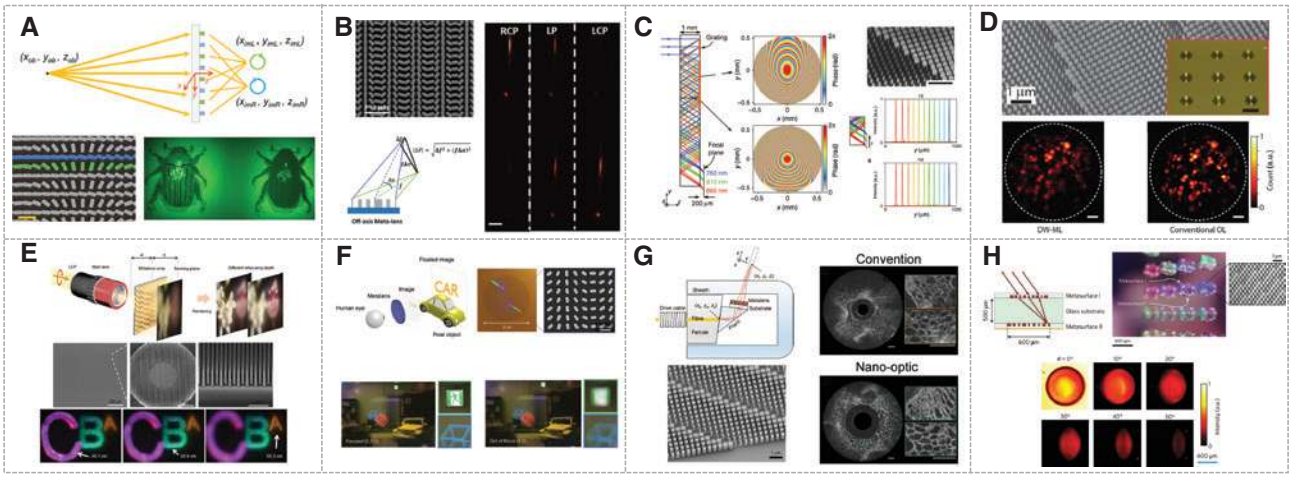

Figure 8: Recent applications of metalenses in devices.
Each figure is arranged in order of mechanism, SEM image, and experimental result. (A) Multispectral chiral imaging with a metalens [144]. (B) Ultracompact visible chiral spectrometer with metalenses [145]. (C) Compact folded metasurface spectrometer [146]. (D) Two-photon microscopy with a double-wavelength metasurface objective lens [147]. (E) Achromatic metalens array for full-color light-field imaging [148]. (F) Metasurface eyepiece for AR [99]. (G) Nano-optic endoscope for high-resolution optical coherence tomography *in vivo* [149]. (H) Planar metasurface retroreflector [150].

from each other, two images can be obtained that form different focuses and also contain chiral information. In Figure 8A, the PB phase-based metalenses are used for chiral imaging to obtain different images when imaging chiral objects [144]. In order to realize such chiral imaging with conventional optics, it is necessary to set up more than two kinds of polarizers and lenses, which shows the strength of the metalens in the compact system.

Metalenses can contribute to compact optical systems because they contain characteristics that are not provided by conventional lenses. Figure 8B and C shows the results of the metalens spectrometer using the dispersive nature of the metasurface [133, 145, 146]. The spectroscopy through the metalens introduced in the Capasso group is implemented through a combination of commercial complementary metal-oxide-semiconductor camera and metalens that has a phase profile in the off-axis focal points [145]. In particular, as it is implemented through the PB phase, it can resolve the helicity of the incident light through a single measurement. Ultimately, this metaspectrometer is encouraging because it was made very compact compared with the existing spectrometer. Figure 8C is a compact and folded metasurface spectrometer recently introduced by the Faraon group [146]. This spectrometer is also characterized by its extremely compact design like the previous study. One of the most important factors for spectroscopic measurements is that the propagation space enough to implement dispersive properties is guaranteed, which is achieved by the realization of the compact folded metasurface. The reliability of the metasurface is further enhanced by these researches because the conventional devices are significantly reduced in size, and with further development, compactness and performance could contribute to the integration of metasurface in real applications.

Metalenses are often applied in some optical systems by replacing the existing lens. In the case of the metalens shown in Figure 8D, the two-photon microscopy is implemented with a metalens [147]. This metalens is a birefringent dual-wavelength metalens, designed to operate at 605 nm wavelength with *x*-polarized light and at 820 nm with *y*-polarized light, and at each wavelength, this metalens has different focal points [79, 147]. Because of the dispersive nature and off-axis coma aberration of metalens, the performance of metalenses in two-photon microscopy was slightly lower than that of conventional lenses. However, the limitation can be further improved with recent metasurface design, and this is well discussed in this paper. As a result, considering the recent developments in metasurface design, it can be said that this study expanded the possibility of metalens-integrated system.

As shown in Figure 8E, a microlens array is fabricated through the previously proposed gallium nitride achromatic metalens and is used for light-field imaging [126, 148]. This study shows that achromatic metalens can be used as a compact planar optical element in a real-life AR imaging device. Considering that the existing light-field imaging system consists of a bulky lens, the compactness

of the entire system can be greatly reduced with metalens. Conversely, the system present at Figure 8F uses the metalens as an eyepiece to greatly improve the performance and reduce the size of the entire system [99]. In the AR system with the metalens, this study has succeeded in greatly improving the field of view, which is one of the persistent problems of conventional AR system, which is difficult to be solved by existing lenses. The example shown in Figure 8G is an example of replacing the ball lens (or graded-index lens) with a metalens in the existing endoscope to improve its performance [149]. Measurement using a conventional system suffers from aberrations including astigmatism, which leads to the degradation of the resultant captured image. In this study, the diffraction-limited focusing with metalens is achieved, and improvement of both depth of focus and transverse resolution is obtained simultaneously, which is also difficult with conventional ball lens or graded-index lens. These two studies ease design tradeoffs because of the ability of the metasurface itself in light control and also have the advantages of compactness when metalenses are applied to real devices. Figure 8H is a planar retroreflector realized by a doublet of metasurface [150]. Instead of a bulky design for an existing retroreflector, this provides a compact planar retroreflector through a freely adjustable phase meta-atom.

4 Outlook

In this review, the metasurfaces are briefly discussed focusing on metahologram and metalens. We briefly summarizes the metasurface holography and lens with some representative studies by their efficiency, modulation features, and operational wavelength in Tables 1 and 2. The functionality is so greatly developed that can be applied in real-life devices, and some prototypes of metasurface-based optical devices are presented as well. Besides the discussed metasurfaces, numerous optical components have been replaced with the metasurfaces that have merits in compactness and performance. Representative examples are polarizer, diffuser, beam deflector, beam splitter, and color filter [33, 34, 151–163]. Recently, with conventional bulk optical elements, it is tricky to output ultracompact devices, because the resultant device cannot help big sizes to have electronic, mechanic, and optical parts as a whole. Accordingly, there are needs for a compact and small-volume platform like metasurface. In this regard, the review discusses the potential of metasurfaces, which are ultrathin elements that can freely control the properties of light, and studies on the enhancement of the functionality of metasurfaces and their practical application to devices are continuing. In addition, most

Table 1: Conclusive table on meta-hologram.

Year	Material	Efficiency[a] (%)	Modulation Feature	Operating space	Operation wavelength (nm)	Ref.
2013	Gold	–	PB phase	Transmission	810	[29]
2013	Gold	~10	Phase (eight levels), amplitude (four levels)	Reflection	676	[32]
2014	Gold	~18	Phase (four levels, polarization control)	Reflection	405–780	[63]
2015	Silicon	~91	Phase (polarization-controlled)	Transmission	915	[20]
2015	Gold	4.5	Phase (holographic multiplexing)	Transmission	633–1000	[50]
2015	Silver	59.2	Phase (holographic multiplexing)	Reflection	620–1020	[39]
2015	Gold	80	PB phase	Reflection	630–1050	[49]
2016	Silicon	75	Phase (polarization multiplexing)	Transmission	460–1800	[64]
2016	Aluminum	2	Phase (full color)	Transmission	420–740	[67]
2016	Gold	3.13	Phase (full color)	Transmission	380–780	[69]
2016	Silicon	~18	Phase (full color)	Transmission	473, 532, 633	[40]
2017	Titanium dioxide	43	Phase (polarization multiplexing)	Transmission	480–633	[19]
2017	Silicon	~46	Phase (incident angle multiplexing)	Reflection	915	[55]
2017	Gold	–	Phase (strain multiplexing)	Transmission	632	[91]
2018	Silver	~30	Phase, polarization	Reflection	650–850	[57]
2018	Silicon	–	Phase, amplitude	Transmission	473–660	[21]
2018	Silicon	~1.18	Amplitude (incident angle multiplexing)	Transmission	470–633	[56]
2018	Gold	6.8	Phase (polarization multiplexing)	Transmission	720–870	[62]
2018	Silicon	~30	Phase (holographic, color)	Transmission	488–633	[70]
2019	Silicon	~26	Phase (full space)	Both	660	[54]
2019	GST	~2	Phase (dynamic)	Transmission	1300–1700	[60]
2019	Chromium	–	Full color, full space	Both	430–750	[66]

[a]This efficiency indicates the hologram generation efficiency, not diffraction efficiency from single meta-atom.

Table 2: Conclusive table on metalens.

Year	Material	Efficiency[a] (%)	NA	Modulation feature	Operation wavelength (nm)	Ref.
2012	Gold	5	0.55	PB phase	740	[110]
2013	Gold	–	0.62	Babinet-inverted	476–676	[109]
2014	Silicon	~75	~0.43	PB phase, grating	490–700	[31]
2015	Silicon	~82	~0.99	Polarization insensitive	1550	[65]
2016	Silicon	70	0.48	Doublet, coma correction	850	[129]
2016	Silicon	~90	~0.7	Multiwavelength, birefringent lens	780, 915	[79]
2016	Silicon	22, 65	0.46	Multiwavelength, polarization-insensitive	915, 1550	[77]
2016	Gold	~6	~0.85	Multiwavelength	600, 785, 980	[113]
2016	Gold	–	0.24	Stretchable substrate, zoom lens	633	[134]
2016	Titanium dioxide	~86	~0.8	PB phase, high efficiency at visible	400–700	[30]
2016	Titanium dioxide	~90	~0.85	Polarization-insensitive at visible	405, 532, 660	[117]
2017	Gallium nitride	~38.3	0.22	PB phase, spatial multiplexing	430, 532, 633	[76]
2017	Titanium dioxide	50	0.44	Doublet, coma correction	532	[130]
2017	Titanium dioxide	~21	0.2	Reflective achromatic	490–550	[18]
2018	Silicon	~76	~0.24	Electrically driven varifocal	632	[135]
2018	Silicon	~50	~0.44	MEMS-tunable	915	[132]
2018	Titanium dioxide	~20	~0.2	Visible achromatic	470–670	[125]
2018	Gallium nitride	~40	0.106	Visible achromatic	400–660	[126]
2019	Titanium dioxide	~30	0.2	Visible achromatic polarization-insensitive	460–700	[128]

[a]This efficiency indicates focusing efficiency, not diffraction efficiency from a single meta-atom.

of recent metasurface studies have been conducted on silicon, gallium nitride, etc., which are also used in semiconductor processing, so it seems that the process will not be a big problem for the pragmatic application.

However, there is still a challenge to actually apply metalenses and metasurfaces to practical devices. Typically, in the case of achromatic metalens in the visible band, which is considered to be the most actively used, it is difficult to realize a meta-atom that can satisfy both long diameter and high numerical aperture. In this regard, the dispersion-engineered metasurface is used as a dispersion corrector in addition to the refractive optics system [164]. The result is desirable in performance, but not sufficiently attractive in compactness. The metasurface, which is considered universally applicable to any optical devices, also has a limitation because it is a passive device and the fabrication cost is not negligible. As mentioned above, there are many problems that need to be solved in order for it to be applied to real-life devices with stretchable substrates and metasurfaces through dynamic materials. Studies have been conducted to use metasurface as color filters and microlens arrays as alternatives, but significant improvements in performance and process fee are needed.

Nonetheless, the metasurface will be enabled at large-area fabrication processes in near-term, thanks to the development of EUV processes and mechanical improvement of future stretchable devices. In comparison with the metasurface hologram study of the early days and the recent meta-atom design method, the modulation capability is not comparable in terms of efficiency and controllability. The number of researches applied to the actual system increases, and most of those accomplished a huge reduction of the size of the system. Added to this, recently, metasurface studies showing the possibility of improving the limit of the existing system has been suggested. Considering this, we are counting on that it is not a remote contingency to meet real-life devices, most of which are composed of metasurfaces.

Acknowledgements: This research was supported by the Basic Science Research Program through the National Research Foundation of Korea (NRF) funded by the Ministry of Science and ICT (2017R1A2B2006676).

References

[1] Chen H-T, Taylor AJ, Yu N. A review of metasurfaces: physics and applications. Rep Prog Phys 2016;79:076401.
[2] Zhang L, Mei S, Huang K, Qiu C-W. Advances in full control of electromagnetic waves with metasurfaces. Adv Opt Mater 2016;4:818–33.
[3] Hsiao H-H, Chu CH, Tsai DP. Fundamentals and applications of metasurfaces. Small Methods 2017;1:1600064.
[4] Kruk S, Kivshar Y. Functional meta-optics and nanophotonics governed by Mie resonances. ACS Photonics 2017;4:2638–49.

[5] Wan W, Gao J, Yang X. Metasurface holograms for holographic imaging. Adv Opt Mater 2017;5:1700541.
[6] Khorasaninejad M, Capasso F. Metalenses: versatile multifunctional photonic components. Science 2017;358:eaam8100.
[7] Genevet P, Capasso F, Aieta F, Khorasaninejad M, Devlin R. Recent advances in planar optics: from plasmonic to dielectric metasurfaces. Optica 2017;4:139–52.
[8] Kamali SM, Arbabi E, Arbabi A, Faraon A. A review of dielectric optical metasurfaces for wavefront control. Nanophotonics 2018;7:1041–68.
[9] Su V-C, Chu CH, Sun G, Tsai DP. Advances in optical metasurfaces: fabrication and applications [Invited]. Opt Express 2018;26:13148–82.
[10] He Q, Sun S, Xiao S, Zhou L. High-efficiency metasurfaces: principles, realizations, and applications. Adv Opt Mater 2018;6:1800415.
[11] Chen M, Kim M, Wong AMH, Eleftheriades GV. Huygens' metasurfaces from microwaves to optics: a review. Nanophotonics 2018;7:1207–31.
[12] Lee G, Sung J, Lee B. Recent advances in metasurface hologram technologies. ETRI J 2019;41:10–22.
[13] Sun S, He Q, Hao J, Xiao S, Zhou L. Electromagnetic metasurfaces: physics and applications. Adv Opt Photonics 2019;11:380–479.
[14] She A, Zhang S, Shian S, Clarke DR, Capasso F. Large area metalenses: design, characterization, and mass manufacturing. Opt Express 2018;26:1573–83.
[15] Glybovski SB, Tretyakov SA, Belov PA, Kivshar YS, Simovski CR. Metasurfaces: from microwaves to visible. Phys Rep 2016;634:1–72.
[16] Yu N, Capasso F. Flat optics with designer metasurfaces. Nat Mater 2014;13:139–50.
[17] Kim I, Yoon G, Jang J, Genevet P, Nam KT, Rho J. Outfitting next generation displays with optical metasurfaces. ACS Photonics 2018;5:3876–95.
[18] Khorasaninejad M, Shi Z, Zhu AY, et al. Achromatic metalens over 60 nm bandwidth in the visible and metalens with reverse chromatic dispersion. Nano Lett 2017;17:1819–24.
[19] Balthasar Mueller JP, Rubin NA, Devlin RC, Groever B, Capasso F. Metasurface polarization optics: independent phase control of arbitrary orthogonal states of polarization. Phys Rev Lett 2017;118:113901.
[20] Arbabi A, Horie Y, Bagheri M, Faraon A. Dielectric metasurfaces for complete control of phase and polarization with subwavelength spatial resolution and high transmission. Nat Nanotechnol 2015;10:937–43.
[21] Lee G-Y, Yoon G, Lee S-Y, et al. Complete amplitude and phase control of light using broadband holographic metasurfaces. Nanoscale 2018;10:4237–45.
[22] Arbabi E, Arbabi A, Kamali SM, Horie Y, Faraon A. Controlling the sign of chromatic dispersion in diffractive optics with dielectric metasurfaces. Optica 2017;4:625–32.
[23] Mun S-E, Yun H, Choi C, Kim S-J, Lee B. Enhancement and switching of Fano resonance in metamaterial. Adv Opt Mater 2018;6:1800545.
[24] Sun S, He Q, Xiao S, Xu Q, Li X, Zhou L. Gradient-index metasurfaces as a bridge linking propagating waves and surface waves. Nat Mater 2012;11:426–31.
[25] Ni X, Emani NK, Kildishev AV, Boltasseva A, Shalaev VM. Broadband light bending with plasmonic nanoantennas. Science 2012;335:427.
[26] Sun S, Yang K-Y, Wang C-M, et al. High-efficiency broadband anomalous reflection by gradient meta-surfaces. Nano Lett 2012;12:6223–9.
[27] Sun W, He Q, Sun S, Zhou L. High-efficiency surface plasmon meta-couplers: concept and microwave-regime realizations. Light Sci Appl 2016;5:e16003.
[28] Luo W, Xiao S, He Q, Sun S, Zhou L. Photonic spin Hall effect with nearly 100% efficiency. Adv Opt Mater 2015;3:1102–8.
[29] Huang L, Chen X, Mühlenbernd H, et al. Three-dimensional optical holography using a plasmonic metasurface. Nat Commun 2013;4:2808.
[30] Khorasaninejad M, Chen WT, Devlin RC, Oh J, Zhu AY, Capasso F. Metalenses at visible wavelengths: diffraction-limited focusing and subwavelength resolution imaging. Science 2016;352:1190–4.
[31] Lin D, Fan P, Hasman E, Brongersma ML. Dielectric gradient metasurface optical elements. Science 2014;345:298–302.
[32] Ni X, Kildishev AV, Shalaev VM. Metasurface holograms for visible light. Nat Commun 2013;4:2807.
[33] Li Z, Palacios E, Butun S, Aydin K. Visible-frequency metasurfaces for broadband anomalous reflection and high-efficiency spectrum splitting. Nano Lett 2015;15:1615–21.
[34] Khorasaninejad M, Zhu W, Crozier KB. Efficient polarization beam splitter pixels based on a dielectric metasurface. Optica 2015;2:376–82.
[35] Lee S-Y, Lee I-M, Park J, et al. Role of magnetic induction currents in nanoslit excitation of surface plasmon polaritons. Phys Rev Lett 2012;108:213907.
[36] Song E-Y, Lee G-Y, Park H, et al. Compact generation of Airy beams with C-aperture metasurface. Adv Opt Mater 2017;5:1601028.
[37] Lee S-Y, Kim K, Kim S-J, Park H, Kim K-Y, Lee B. Plasmonic meta-slit: shaping and controlling near-field focus. Optica 2015;2:6–13.
[38] Lee G-Y, Lee S-Y, Yun H, et al. Near-field focus steering along arbitrary trajectory via multi-lined distributed nanoslits. Sci Rep 2016;6:33317.
[39] Wen D, Yue F, Li G, et al. Helicity multiplexed broadband metasurface holograms. Nat Commun 2015;6:8241.
[40] Wang B, Dong F, Li Q-T, et al. Visible-frequency dielectric metasurfaces for multiwavelength achromatic and highly dispersive holograms. Nano Lett 2016;16:5235–40.
[41] Liu S, Vabishchevich PP, Vaskin A, et al. An all-dielectric metasurface as a broadband optical frequency mixer. Nat Commun 2018;9:2507.
[42] Li Z, Dai Q, Mehmood MQ, et al. Full-space cloud of random points with a scrambling metasurface. Light Sci Appl 2018;7:63.
[43] Jang M, Horie Y, Shibukawa A, et al. Wavefront shaping with disorder-engineered metasurfaces. Nat Photonics 2018;12:84–90.
[44] Maguid E, Yulevich I, Yannai M, Kleiner V, Brongersma ML, Hasman E. Multifunctional interleaved geometric-phase dielectric metasurfaces. Light Sci Appl 2017;6:e17027.
[45] Hariharan P. Optical holography: principles, techniques, and applications, 2nd ed. New York, NY: Cambridge University Press, 1996.
[46] Goodman JW. Introduction to Fourier optics, 2nd ed. New York, NY: McGraw-Hill, 1996.

[47] Günter P. Holography, coherent light amplification and optical phase conjugation with photorefractive materials. Phys Rep 1982;93:199–299.
[48] Blanche P-A, Bablumian A, Voorakaranam R, et al. Holographic three-dimensional telepresence using large-area photorefractive polymer. Nature 2010;468:80–3.
[49] Zheng G, Mühlenbernd H, Kenney M, Li G, Zentgraf T, Zhang S. Metasurface holograms reaching 80% efficiency. Nat Nanotechnol 2015;10:308–12.
[50] Huang L, Mühlenbernd H, Li X, et al. Broadband hybrid holographic multiplexing with geometric metasurfaces. Adv Mater 2015;27:6444–9.
[51] Xiao D, Chang M-C, Niu Q. Berry phase effects on electronic properties. Rev Mod Phys 2010;82:1959–2007.
[52] Zhao R, Sain B, Wei Q, et al. Multichannel vectorial holographic display and encryption. Light Sci Appl 2018;7:95.
[53] Zhang F, Pu M, Li X, et al. All-Dielectric metasurfaces for simultaneous giant circular asymmetric transmission and wavefront shaping based on asymmetric photonic spin-orbit interactions. Adv Funct Mater 2017;27:1704295.
[54] Sung J, Lee G, Choi C, Hong J, Lee B. Single-layer bifacial metasurface: full-space visible light control. Adv Opt Mater 2019;7:1801748.
[55] Kamali SM, Arbabi E, Arbabi A, Horie Y, Faraji-Dana M, Faraon A. Angle-multiplexed metasurfaces: encoding independent wavefronts in a single metasurface under different illumination angles. Phys Rev X 2017;7:041056.
[56] Bao Y, Yu Y, Xu H, et al. Coherent pixel design of metasurfaces for multidimensional optical control of multiple printing-image switching and encoding. Adv Funct Mater 2018;28:1805306.
[57] Deng Z-L, Deng J, Zhuang X, et al. Diatomic metasurface for vectorial holography. Nano Lett 2018;18:2885–92.
[58] Chen Y, Yang X, Gao J. 3D Janus plasmonic helical nanoapertures for polarization-encrypted data storage. Light Sci Appl 2019;8:45.
[59] Guo Y, Huang Y, Li X, et al. Polarization-controlled broadband accelerating beams generation by single catenary-shaped metasurface. Adv Opt Mater 2019. doi:10.1002/adom.201900503.
[60] Choi C, Lee S, Mun S, et al. Metasurface with nanostructured $Ge_2Sb_2Te_5$ as a platform for broadband-operating wavefront switch. Adv Opt Mater 2019;7:1900171.
[61] Kruk S, Hopkins B, Kravchenko II, Miroshnichenko A, Neshev DN, Kivshar YS. Invited Article: Broadband highly efficient dielectric metadevices for polarization control. APL Photonics 2016;1:030801.
[62] Chen Y, Yang X, Gao J. Spin-controlled wavefront shaping with plasmonic chiral geometric metasurfaces. Light Sci Appl 2018;7:84.
[63] Chen WT, Yang K-Y, Wang C-M, et al. High-efficiency broadband meta-hologram with polarization-controlled dual images. Nano Lett 2014;14:225–30.
[64] Khorasaninejad M, Ambrosio A, Kanhaiya P, Capasso F. Broadband and chiral binary dielectric meta-holograms. Sci Adv 2016;2:e1501258.
[65] Arbabi A, Horie Y, Ball AJ, Bagheri M, Faraon A. Subwavelength-thick lenses with high numerical apertures and large efficiency based on high-contrast transmitarrays. Nat Commun 2015;6:7069.
[66] Zhang X, Pu M, Guo Y, et al. Colorful metahologram with independently controlled images in transmission and reflection spaces. Adv Funct Mater 2019;29:1809145.
[67] Wan W, Gao J, Yang X. Full-color plasmonic metasurface holograms. ACS Nano 2016;10:10671–80.
[68] Qiu M, Jia M, Ma S, Sun S, He Q, Zhou L. Angular dispersions in terahertz metasurfaces: physics and applications. Phys Rev Appl 2018;9:054050.
[69] Li X, Chen L, Li Y, et al. Multicolor 3D meta-holography by broadband plasmonic modulation. Sci Adv 2016;2:e1601102.
[70] Jin L, Dong Z, Mei S, et al. Noninterleaved metasurface for (2 6 –1) spin- and wavelength-encoded holograms. Nano Lett 2018;18:8016–24.
[71] Wu PC, Tsai W-Y, Chen WT, et al. Versatile polarization generation with an aluminum plasmonic metasurface. Nano Lett 2017;17:445–52.
[72] Shi Z, Khorasaninejad M, Huang Y-W, et al. Single-layer metasurface with controllable multiwavelength functions. Nano Lett 2018;18:2420–7.
[73] Zang X, Dong F, Yue F, et al. Polarization encoded color image embedded in a dielectric metasurface. Adv Mater 2018;30:1707499.
[74] Huang Y-W, Chen WT, Tsai W-Y, et al. Aluminum plasmonic multicolor meta-hologram. Nano Lett 2015;15:3122–7.
[75] Dong F, Feng H, Xu L, et al. Information encoding with optical dielectric metasurface via independent multichannels. ACS Photonics 2019;6:230–7.
[76] Chen BH, Wu PC, Su V-C, et al. GaN metalens for pixel-level full-color routing at visible light. Nano Lett 2017;17:6345–52.
[77] Arbabi E, Arbabi A, Kamali SM, Horie Y, Faraon A. Multiwavelength polarization-insensitive lenses based on dielectric metasurfaces with meta-molecules. Optica 2016;3:628–33.
[78] Arbabi E, Arbabi A, Kamali SM, Horie Y, Faraon A. Multiwavelength metasurfaces through spatial multiplexing. Sci Rep 2016;6:32803.
[79] Arbabi E, Arbabi A, Kamali SM, Horie Y, Faraon A. High efficiency double-wavelength dielectric metasurface lenses with dichroic birefringent meta-atoms. Opt Express 2016;24:18468–77.
[80] Zhang M, Pu M, Zhang F, et al. Plasmonic metasurfaces for switchable photonic spin-orbit interactions based on phase change materials. Adv Sci 2018;5:1800835.
[81] Li J, Kamin S, Zheng G, Neubrech F, Zhang S, Liu N. Addressable metasurfaces for dynamic holography and optical information encryption. Sci Adv 2018;4:eaar6768.
[82] Yu P, Li J, Zhang S, et al. Dynamic Janus metasurfaces in the visible spectral region. Nano Lett 2018;18:4584–9.
[83] Forouzmand A, Salary MM, Inampudi S, Mosallaei H. A tunable multigate indium-tin-oxide-assisted all-dielectric metasurface. Adv Opt Mater 2018;6:1701275.
[84] Hashemi MRM, Yang S-H, Wang T, Sepúlveda N, Jarrahi M. Electronically-controlled beam-steering through vanadium dioxide metasurfaces. Sci Rep 2016;6:35439.
[85] Huang Y-W, Lee HWH, Sokhoyan R, et al. Gate-tunable conducting oxide metasurfaces. Nano Lett 2016;16:5319–25.
[86] Kafaie Shirmanesh G, Sokhoyan R, Pala RA, Atwater HA. Dual-gated active metasurface at 1550 nm with wide (>300°) phase tunability. Nano Lett 2018;18:2957–63.
[87] Komar A, Paniagua-Domínguez R, Miroshnichenko A, et al. Dynamic beam switching by liquid crystal tunable dielectric metasurfaces. ACS Photonics 2018;5:1742–8.
[88] Zou C, Komar A, Fasold S, et al. Electrically tunable transparent displays for visible light based on dielectric metasurfaces. ACS Photonics 2019;6:1533–40.

[89] Park J-W, Eom SH, Lee H, et al. Optical properties of pseudobinary GeTe, $Ge_2Sb_2Te_5$, $GeSb_2Te_4$, $GeSb_4Te_7$, and Sb_2Te_3 from ellipsometry and density functional theory. Phys Rev B 2009;80:115209.
[90] Raoux S. Phase change materials. Annu Rev Mater Res 2009;39:25–48.
[91] Malek SC, Ee H-S, Agarwal R. Strain multiplexed metasurface holograms on a stretchable substrate. Nano Lett 2017;17:3641–5.
[92] Cai T, Tang S, Wang G, et al. High-performance bifunctional metasurfaces in transmission and reflection geometries. Adv Opt Mater 2017;5:1600506.
[93] Cai T, Wang G, Tang S, et al. High-efficiency and full-space manipulation of electromagnetic wave fronts with metasurfaces. Phys Rev Appl 2017;8:034033.
[94] Zhang L, Wu RY, Bai GD, et al. Transmission-reflection-integrated multifunctional coding metasurface for full-space controls of electromagnetic waves. Adv Funct Mater 2018;28:1802205.
[95] Zhu AY, Chen WT, Zaidi A, et al. Giant intrinsic chiro-optical activity in planar dielectric nanostructures. Light Sci Appl 2018;7:17158.
[96] Li Z, Liu W, Cheng H, Chen S, Tian J. Spin-selective transmission and devisable chirality in two-layer metasurfaces. Sci Rep 2017;7:8204.
[97] Yun J-G, Kim S-J, Yun H, et al. Broadband ultrathin circular polarizer at visible and near-infrared wavelengths using a non-resonant characteristic in helically stacked nano-gratings. Opt Express 2017;25:14260.
[98] Mun S-E, Hong J, Yun J-G, Lee B. Broadband circular polarizer for randomly polarized light in few-layer metasurface. Sci Rep 2019;9:2543.
[99] Lee G-Y, Hong J-Y, Hwang S, et al. Metasurface eyepiece for augmented reality. Nat Commun 2018;9:4562.
[100] Jang C, Bang K, Li G, Lee B. Holographic near-eye display with expanded eye-box. ACM Trans Graph 2018;37:1–14.
[101] Lee S, Jo Y, Yoo D, Cho J, Lee D, Lee B. Tomographic near-eye displays. Nat Commun 2019;10:2497.
[102] Lalanne P, Chavel P. Metalenses at visible wavelengths: past, present, perspectives. Laser Photonics Rev 2017;11:1600295.
[103] Hasman E, Kleiner V, Biener G, Niv A. Polarization dependent focusing lens by use of quantized Pancharatnam–Berry phase diffractive optics. Appl Phys Lett 2003;82:328–30.
[104] Paniagua-Domínguez R, Yu YF, Khaidarov E, et al. A metalens with a near-unity numerical aperture. Nano Lett 2018;18:2124–32.
[105] Zuo H, Choi D-Y, Gai X, et al. High-efficiency all-dielectric metalenses for mid-infrared imaging. Adv Opt Mater 2017;5:1700585.
[106] Tseng ML, Hsiao H-H, Chu CH, et al. Metalenses: advances and applications. Adv Opt Mater 2018;6:1800554.
[107] Wang W, Guo Z, Li R, et al. Ultra-thin, planar, broadband, dual-polarity plasmonic metalens. Photonics Res 2015;3:68–71.
[108] Wang W, Guo Z, Li R, et al. Plasmonics metalens independent from the incident polarizations. Opt Express 2015;23:16782–91.
[109] Ni X, Ishii S, Kildishev AV, Shalaev VM. Ultra-thin, planar, Babinet-inverted plasmonic metalenses. Light Sci Appl 2013;2:e72.
[110] Chen X, Huang L, Mühlenbernd H, et al. Dual-polarity plasmonic metalens for visible light. Nat Commun 2012;3:1198.
[111] Chen X, Huang L, Mühlenbernd H, et al. Reversible three-dimensional focusing of visible light with ultrathin plasmonic flat lens. Adv Opt Mater 2013;1:517–21.
[112] Wang S, Wu PC, Su V-C, et al. Broadband achromatic optical metasurface devices. Nat Commun 2017;8:187.
[113] Hu J, Liu C-H, Ren X, Lauhon LJ, Odom TW. Plasmonic lattice lenses for multiwavelength achromatic focusing. ACS Nano 2016;10:10275–82.
[114] Williams C, Montelongo Y, Wilkinson TD. Plasmonic metalens for narrowband dual-focus imaging. Adv Opt Mater 2017;5:1700811.
[115] Li X, Xiao S, Cai B, He Q, Cui TJ, Zhou L. Flat metasurfaces to focus electromagnetic waves in reflection geometry. Opt Lett 2012;37:4940–2.
[116] West PR, Stewart JL, Kildishev AV, et al. All-dielectric subwavelength metasurface focusing lens. Opt Express 2014;22:26212.
[117] Khorasaninejad M, Zhu AY, Roques-Carmes C, et al. Polarization-insensitive metalenses at visible wavelengths. Nano Lett 2016;16:7229–34.
[118] Boroviks S, Deshpande RA, Mortensen NA, Bozhevolnyi SI. Multifunctional metamirror: polarization splitting and focusing. ACS Photonics 2018;5:1648–53.
[119] Wen D, Yue F, Ardron M, Chen X. Multifunctional metasurface lens for imaging and Fourier transform. Sci Rep 2016;6:27628.
[120] Chen X, Chen M, Mehmood MQ, et al. Longitudinal multifoci metalens for circularly polarized light. Adv Opt Mater 2015;3:1201–6.
[121] Zhang Z, Wen D, Zhang C, et al. Multifunctional light sword metasurface lens. ACS Photonics 2018;5:1794–9.
[122] Groever B, Rubin NA, Mueller JPB, Devlin RC, Capasso F. High-efficiency chiral meta-lens. Sci Rep 2018;8:7240.
[123] Hu J, Wang D, Bhowmik D, et al. Lattice-resonance metalenses for fully reconfigurable imaging. ACS Nano 2019;13:4613–20.
[124] Colburn S, Zhan A, Majumdar A. Metasurface optics for full-color computational imaging. Sci Adv 2018;4:eaar2114.
[125] Chen WT, Zhu AY, Sanjeev V, et al. A broadband achromatic metalens for focusing and imaging in the visible. Nat Nanotechnol 2018;13:220–6.
[126] Wang S, Wu PC, Su V-C, et al. A broadband achromatic metalens in the visible. Nat Nanotechnol 2018;13:227–32.
[127] Shrestha S, Overvig AC, Lu M, Stein A, Yu N. Broadband achromatic dielectric metalenses. Light Sci Appl 2018;7:85.
[128] Chen WT, Zhu AY, Sisler J, Bharwani Z, Capasso F. A broadband achromatic polarization-insensitive metalens consisting of anisotropic nanostructures. Nat Commun 2019;10:355
[129] Arbabi A, Arbabi E, Kamali SM, Horie Y, Han S, Faraon A. Miniature optical planar camera based on a wide-angle metasurface doublet corrected for monochromatic aberrations. Nat Commun 2016;7:13682.
[130] Groever B, Chen WT, Capasso F. Meta-lens doublet in the visible region. Nano Lett 2017;17:4902–7.
[131] She A, Zhang S, Shian S, Clarke DR, Capasso F. Adaptive metalenses with simultaneous electrical control of focal length, astigmatism, and shift. Sci Adv 2018;4:eaap9957.
[132] Arbabi E, Arbabi A, Kamali SM, Horie Y, Faraji-Dana M, Faraon A. MEMS-tunable dielectric metasurface lens. Nat Commun 2018;9:812.
[133] Zhu AY, Chen WT, Sisler J, et al. Compact aberration-corrected spectrometers in the visible using dispersion-tailored metasurfaces. Adv Opt Mater 2018;7:1801144.

[134] Ee H-S, Agarwal R. Tunable metasurface and flat optical zoom lens on a stretchable substrate. Nano Lett 2016;16:2818–23.
[135] Afridi A, Canet-Ferrer J, Philippet L, Osmond J, Berto P, Quidant R. Electrically driven varifocal silicon metalens. ACS Photonics 2018;5:4497–503.
[136] Roy T, Zhang S, Jung IW, Troccoli M, Capasso F, Lopez D. Dynamic metasurface lens based on MEMS technology. APL Photonics 2018;3:021302.
[137] Papaioannou M, Plum E, Rogers ET, Zheludev NI. All-optical dynamic focusing of light via coherent absorption in a plasmonic metasurface. Light Sci Appl 2018;7:17157.
[138] Liu X, Deng J, Li KF, et al. Optical metasurfaces for designing planar Cassegrain-Schwarzschild objectives. Phys Rev Appl 2019;11:054055.
[139] Yesilkoy F, Arvelo ER, Jahani Y, et al. Ultrasensitive hyperspectral imaging and biodetection enabled by dielectric metasurfaces. Nat Photonics 2019;13:390–6.
[140] Li L, Ruan H, Liu C, et al. Machine-learning reprogrammable metasurface imager. Nat Commun 2019;10:1082.
[141] Holsteen AL, Lin D, Kauvar I, Wetzstein G, Brongersma ML. A light-field metasurface for high-resolution single-particle tracking. Nano Lett 2019;19:2267–71.
[142] Yang J, Ghimire I, Wu PC, et al. Photonic crystal fiber metalens. Nanophotonics 2019;8:443–9.
[143] Lan S, Zhang X, Taghinejad M, et al. Metasurfaces for near-eye augmented reality. ACS Photonics 2019;6:864–70.
[144] Khorasaninejad M, Chen WT, Zhu AY, et al. Multispectral chiral imaging with a metalens. Nano Lett 2016;16:4595–600.
[145] Zhu AY, Chen W-T, Khorasaninejad M, et al. Ultra-compact visible chiral spectrometer with meta-lenses. APL Photonics 2017;2:036103.
[146] Faraji-Dana M, Arbabi E, Arbabi A, Kamali SM, Kwon H, Faraon A. Compact folded metasurface spectrometer. Nat Commun 2018;9:4196.
[147] Arbabi E, Li J, Hutchins RJ, et al. Two-photon microscopy with a double-wavelength metasurface objective lens. Nano Lett 2018;18:4943–8.
[148] Lin RJ, Su V-C, Wang S, et al. Achromatic metalens array for full-colour light-field imaging. Nat Nanotechnol 2019;14:227–31.
[149] Pahlevaninezhad H, Khorasaninejad M, Huang Y-W, et al. Nano-optic endoscope for high-resolution optical coherence tomography in vivo. Nat Photonics 2018;12:540–7.
[150] Arbabi A, Arbabi E, Horie Y, Kamali SM, Faraon A. Planar metasurface retroreflector. Nat Photonics 2017;11:415–20.
[151] Balthasar Mueller JP, Leosson K, Capasso F. Ultracompact metasurface in-line polarimeter. Optica 2016;3:42.
[152] Chen WT, Török P, Foreman MR, et al. Integrated plasmonic metasurfaces for spectropolarimetry. Nanotechnology 2016;27:224002.
[153] Arbabi E, Kamali SM, Arbabi A, Faraon A. Full-Stokes imaging polarimetry using dielectric metasurfaces. ACS Photonics 2018;5:3132–40.
[154] Lee K, Yun H, Mun S-E, Lee G-Y, Sung J, Lee B. Ultracompact broadband plasmonic polarimeter. Laser Photonics Rev 2018;12:1700297.
[155] Wu PC, Chen J-W, Yin C-W, et al. Visible metasurfaces for on-chip polarimetry. ACS Photonics 2018;5:2568–73.
[156] Yang Z, Wang Z, Wang Y, et al. Generalized Hartmann-Shack array of dielectric metalens sub-arrays for polarimetric beam profiling. Nat Commun 2018;9:4607.
[157] Shalaev MI, Sun J, Tsukernik A, Pandey A, Nikolskiy K, Litchinitser NM. High-efficiency all-dielectric metasurfaces for ultracompact beam manipulation in transmission mode. Nano Lett 2015;15:6261–6.
[158] Yu YF, Zhu AY, Paniagua-Domínguez R, Fu YH, Luk'yanchuk B, Kuznetsov AI. High-transmission dielectric metasurface with 2π phase control at visible wavelengths. Laser Photonics Rev 2015;9:412–8.
[159] Hong J, Kim S-J, Kim I, et al. Plasmonic metasurface cavity for simultaneous enhancement of optical electric and magnetic fields in deep subwavelength volume. Opt Express 2018;26:13340–8.
[160] Qin F, Ding L, Zhang L, et al. Hybrid bilayer plasmonic metasurface efficiently manipulates visible light. Sci Adv 2016;2:e1501168.
[161] Kita S, Takata K, Ono M, et al. Coherent control of high efficiency metasurface beam deflectors with a back partial reflector. APL Photonics 2017;2:046104.
[162] Zhou Z, Li J, Su R, et al. Efficient silicon metasurfaces for visible light. ACS Photonics 2017;4:544–51.
[163] Wang B, Dong F, Feng H, et al. Rochon-prism-like planar circularly polarized beam splitters based on dielectric metasurfaces. ACS Photonics 2018;5:1660–4.
[164] Chen WT, Zhu AY, Sisler J, et al. Broadband achromatic metasurface-refractive optics. Nano Lett 2018;18:7801–8.